Electrochemical Properties and Applications of Nanocrystalline, Microcrystalline, and Epitaxial Cubic Silicon Carbide Films

Hao Zhuang, Nianjun Yang, Lei Zhang, Regina Fuchs, and Xin Jiang*

Institute of Materials Engineering, University of Siegen, Paul-Bonatz-Strasse 9-11, 57076 Siegen, Germany

Ⓢ Supporting Information

ABSTRACT: Microstructures of the materials (e.g., crystallinitiy, defects, and composition, etc.) determine their properties, which eventually lead to their diverse applications. In this contribution, the properties, especially the electrochemical properties, of cubic silicon carbide (3C-SiC) films have been engineered by controlling their microstructures. By manipulating the deposition conditions, nanocrystalline, microcrystalline and epitaxial (001) 3C-SiC films are obtained with varied properties. The epitaxial 3C-SiC film presents the lowest double-layer capacitance and the highest reversibility of redox probes, because of its perfect (001) orientation and high phase purity. The highest double-layer capacitance and the lowest reversibility of redox probes have been realized on the nanocrystalline 3C-SiC film. Those are ascribed to

its high amount of grain boundaries, amorphous phases and large diversity in its crystal size. Based on their diverse properties, the electrochemical performances of 3C-SiC films are evaluated in two kinds of potential applications, namely an electrochemical capacitor using a nanocrystalline film and an electrochemical dopamine sensor using the epitaxial 3C-SiC film. The nanocrystalline 3C-SiC film shows not only a high double layer capacitance ($43-70\ \mu F/cm^2$) but also a long-term stability of its capacitance. The epitaxial 3C-SiC film shows a low detection limit toward dopamine, which is one to 2 orders of magnitude lower than its normal concentration in tissue. Therefore, 3C-SiC film is a novel but designable material for different emerging electrochemical applications such as energy storage, biomedical/chemical sensors, environmental pollutant detectors, and so on.

KEYWORDS: silicon carbide, thin film, electrochemistry, structural design, super capacitor, sensor
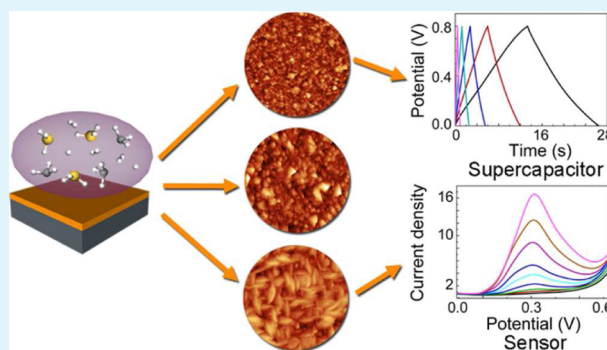
1. INTRODUCTION

Through engineering the microstructure (e.g., crystallinitiy, defects, composition, etc.) of a material, its basic properties can be manipulated which in turn lead to its diverse performance.[1] As a result, emerging applications have been continuously explored from traditional materials. For instance, diamond has recently been employed in high-performance biosensors[2,3] and quantum computer applications[4] besides its conventional usage in industrial drills; understanding the electrical conductivity of polymers has made the flexible display possible,[5] and so on.

Silicon carbide (SiC), a famous traditional material, has been considered of great technical importance since the 1890s, soon after its successful commercial production.[6] Because of its high hardness and good chemical stability, it was utilized at the beginning only as the abrasive. Later on, the successful wafer scale production of single-crystalline SiC widened its applications nowadays in semiconductor industry,[7] mainly as substrates for high temperature and high power electronics.[8] Nevertheless, because of its combined advantages of high chemical stability, high electron mobility (cubic polytype), good mechanical robustness, diverse surface chemistry, good biocompatibility, etc., its potential is being continuously exploited.[9-12] Its cubic polytype, denoted as 3C-SiC, has been demonstrated recently as a novel electrode in electro-

chemistry.[13-15] Meanwhile, it is well-known that 3C-SiC can be synthesized with different forms, i.e., bulk crystals,[7] thin films,[16] (zero-dimensional) nanoparticles,[17] (one-dimensional) nanowires,[18] and (two-dimensional) nanosheets.[19] These different forms lead to their diverse physical and chemical properties.[20,21] In this context, before its full implementation, the relationship between the properties and the microstructures (i.e., crystallinity, defects, composition, etc.) of SiC needs to be well-understood. Following this argument, in the present study, we systematically studied the influence of microstructure (i.e., crystallinity, defects, composition, etc.) on the electrochemical properties of 3C-SiC films. We controlled the microstructure of the 3C-SiC films by means of manipulating their deposition conditions in the chemical vapor deposition (CVD) process. The different microstructures in turn lead to their diverse electrochemical properties. On the basis of their properties, the 3C-SiC films are believed to be applicable in various electrochemical applications. In order to shed some light on their possible future applications, the performance of 3C-SiC films in two example electrochemical applications are

Table 1. Deposition Parameters and Characteristic Properties of the 3C-SiC Films

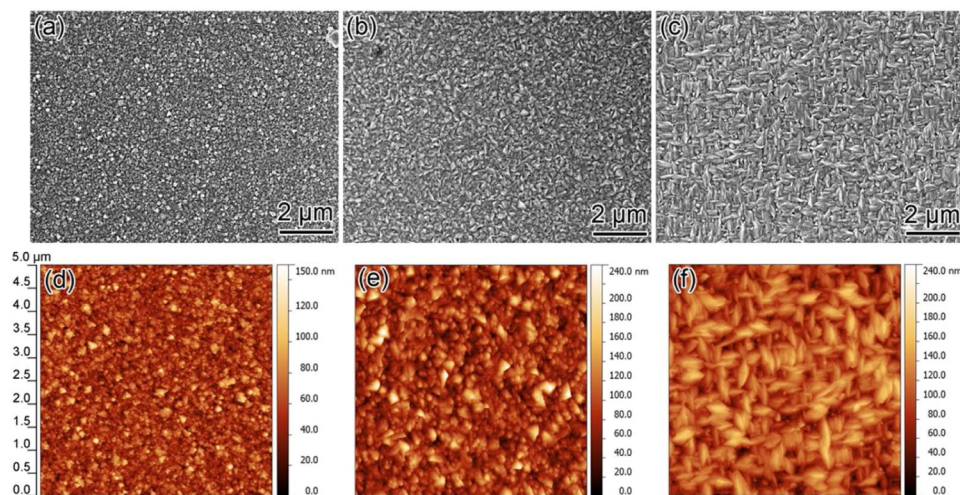| film type	MW power (W)	gas pressure (Torr)	T_s (°C)	TMS content (ppm)	thickness (nm)	growth rate (nm/h)	surface roughness (R_a, nm)	sheet resistance (Ω/sq)
nanocryst.	700	20	~800	290	700	~120	12.6	3316 ± 76
microcryst.	1800	45	~700	290	580	~100	22.9	3392 ± 220
epitaxial	2200	55	~850	140	300	~50	20.6	86 ± 7

Figure 1. (a–c) SEM surface and (d–f) AFM noncontact mode images of (a, d) nanocrystalline, (b, e) microcrystalline, and (c, f) epitaxial 3C-SiC films. The size of the AFM images is 5 μm × 5 μm.

demonstrated: (1) using the nanocrystalline 3C-SiC film as a substrate for supercapacitor and (2) the epitaxial (001) 3C-SiC film as an electrode for sensing.

2. EXPERIMENTAL SECTION

Chemicals. H_2SO_4, H_2O_2 (35%), ferrocene, NaH_2PO_4, Na_2HPO_4, $K_4Fe(CN)_6$, $K_3Fe(CN)_6$, $Ru(NH_3)_6Cl_3$, dopamine hydrochloride, tetra-*n*-butylammonium tetrafluoroborate ($TBABF_4$), and acetonitrile were obtained from Alfa Aesar. HF (≥48%), p-benzoquinone, and KCl are purchased from Sigma-Aldrich. All chemicals are used as purchased. Dopamine solutions with concentrations ranging from 2 μM to 200 μM are prepared by dissolving dopamine hydrochloride in 0.1 M phosphate buffer (pH 7.4). All the aqueous solutions are prepared using Milli-Q water.

Preparation of 3C-SiC Films. The 3C-SiC films were grown on single-crystalline (100) Si substrates using microwave plasma chemical vapor deposition technique. The reactive gas features a mixture of H_2 and tetramethylsilane (TMS). By varying the deposition parameters, i.e., microwave power, gas pressure, substrate temperature (monitored by an optical pyrometer) and gas phase composition, 3C-SiC films with different structures can be obtained. Table 1 listed the detailed deposition conditions for the nanocrystalline, microcrystalline and epitaxial 3C-SiC films used in the present study.

Structural Characterization. Scanning electron microscope (SEM, Zeiss Ultra 55) was used to obtain the plane and cross-sectional microstructures of the samples. To determine the phase composition and orientation of the samples as well as their variation with different deposition conditions, we performed X-ray diffraction (XRD, PW3040 X'Pert MPD) measurements in the 2θ range of 34–105° with a step size of 0.05°. The standard JPCDS card (No. 29–1129) was used for indexing the observed diffraction peaks. The spectra in the 2θ range of 65–75° are excluded due to the strong Si (400) diffraction peak. Micro Raman scattering studies are carried out to understand the phase purity of the films. The 532 nm line of a Nd:YVO₄ diode-pumped solid-state laser was used as the excitation source. Transmission electron microscopy (TEM, Philips CM20 and Tecnai G2 F20) was utilized to acquire crystal information on the 3C-SiC films.

Electrochemical Measurements. Before the electrochemical measurements, the 3C-SiC films are first cleaned in piranha solution (H_2SO_4:H_2O_2 = 3:1) to remove any inorganic or organic contaminations on the surface. Afterward, the wafer is dipped into 5% HF solution for 3 min to remove the SiO_2 surface layer followed by ultrasonic cleaning in distilled water, rendering OH-terminated 3C-SiC surface.[22] All the electrochemical measurements are carried out on a potentiostat (CHI 660E). A three-electrode configuration with 3C-SiC film as the working electrode, platinum wire as counter electrode and Ag/AgCl (3 M KCl) as the reference electrode was used in the present study. Standard cyclic voltammetry was used to evaluate the performance of the 3C-SiC films in different redox solutions. Differential pulse voltammetry was applied for the detection of dopamine on the 3C-SiC electrode with the following parameters: a pulse height of 50 mV, a step height of 2 mV, a pulse width of 50 ms, and a cycle period of 100 ms.

3. RESULTS AND DISCUSSION

3.1. Structures of the SiC Films. In the present study, microwave plasma chemical vapor deposition (MWCVD) technique was employed for the fabrication of 3C-SiC films. The detailed deposition conditions for the films are listed in Table 1. Three kinds of 3C-SiC films have been grown, namely nanocrystalline, microcrystalline and epitaxial (001) 3C-SiC films. Figure 1 shows the scanning electron microscopy (SEM) and atomic force microscopy (AFM) images of the surface of all the films. As depicted in Figure 1a, the nanocrystalline 3C-SiC film possesses a crystal size smaller than 50 nm. Its surface is relatively smooth and has a root-mean-square (RMS) roughness of only 12.6 nm, as estimated from its AFM noncontact mode image shown in Figure 1d. The average crystal size of the microcrystalline 3C-SiC film is ~200 nm (see Figures 1b and 3b in the following). The larger crystal size together with the low full width at half-maximum (fwhm) of its SiC transverse optical (TO) Raman peak (see Figure 2b in the following) leads to the conclusion that the microcrystalline 3C-
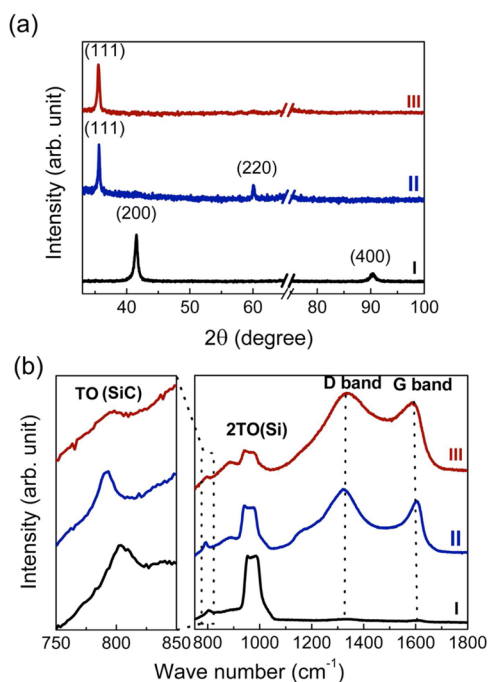
Figure 2. (a) XRD patterns and (b) Raman spectra of (I) epitaxial, (II) microcrystalline, and (III) nanocrystalline 3C-SiC films.

SiC film has a much better crystallinity in comparison with the nanocrystalline 3C-SiC film. Its larger crystal size results in its higher surface roughness, which is measured to be 22.9 nm from the AFM image (Figure 1e). The SEM image of the epitaxial 3C-SiC film is shown in Figure 1c. Densely packed 3C-SiC crystals lying along the ⟨110⟩ directions of the Si wafer is observable, presenting a very typical nature of the hetero-epitaxially grown 3C-SiC crystals on (001) Si.[16,23] Its surface roughness is comparable to that of the microcrystalline 3C-SiC film, which is 20.6 nm determined by the AFM measurement (Figure 1f). The cross-sectional SEM images of the samples are shown in Figure S1 in the Supporting Information. The thicknesses and growth rates of the films were obtained and have been summarized in Table 1.

From Table 1, it can be seen that the change in the morphology of the above films was achieved by controlling the microwave power, gas pressure and the concentration of TMS (the precursor for the growth of 3C-SiC in the present study) during deposition. The mechanism for the above variation has been discussed in detail in one of our previous publications.[16] Briefly, at low microwave power and high TMS concentrations, nanocrystalline 3C-SiC films form because of the high secondary nucleation rate. An increase of the microwave power enhances the concentration of atomic hydrogen in the plasma. In MWCVD, the atomic hydrogen is an important species in determining the crystallinity of the film.[16,24] It removes the defects and amorphous phase in the film through a continuous etching process.[16,24] The higher the concentration of atomic hydrogen, the stronger the etching will be. Since the defects and amorphous phase could serve as the sites for secondary nucleation, their effective removal could in turn improve the crystallinity of the 3C-SiC films.[16,24] As a result, microcrystalline 3C-SiC film with larger crystal size and higher crystal quality forms at high microwave powers. Further increase in the microwave power and decrease of the TMS

concentration lead to the epitaxial growth of the 3C-SiC film on the (001) Si wafer.[16]

More detailed information about the composition of the films has been revealed by the X-ray diffraction (XRD) and Raman measurements. Figure 2a presents the XRD patterns of the above films. Peaks positioning at 35.6, 41.4, 60.0, and 90.0° are indexed to the (111), (200), (220), and (400) reflexes of 3C-SiC, respectively, indicating the formation of 3C-SiC in all films. However, certain differences are still observable. For both nanocrystalline and microcrystalline 3C-SiC films, strong (111) reflex exists. Weak (220) reflex is observed in the microcrystalline 3C-SiC film, indicating its polycrystalline nature. The intensity of the (220) reflex is much weaker in the nanocrystalline 3C-SiC film. For the epitaxial 3C-SiC film, only (200) and (400) reflexes present, indicating its perfect (001) orientation.

Except for the 3C-SiC crystals, it is well understood that amorphous phases normally exist at the grain boundaries during the CVD production of 3C-SiC films.[16] To access this information on our 3C-SiC films, micro-Raman analysis was carried out. Figure 2b shows the obtained Raman spectra. For all films considered, the characteristic Raman peak at ∼800 cm^{-1} is observable, corresponding to the TO phonon of SiC. This peak confirms the formation of SiC in all samples. The fwhm of the SiC TO peaks are >40, 17 and 26 cm^{-1} for nanocrystalline, microcrystalline and epitaxy 3C-SiC films, respectively. The sharper SiC TO peak of the microcrystalline and epitaxial 3C-SiC films in comparison to that of the nanocrystalline 3C-SiC film indicates their better crystallinity. In addition to the SiC TO band, peaks corresponding to the existence of amorphous carbon phase are also observable at ∼1320 cm^{-1} (D band) and ∼1600 cm^{-1} (G band) in the nanocrystalline and microcrystalline 3C-SiC films. Such a phenomenon hints the existence of the amorphous carbon phase in both films. Nevertheless, since the Raman efficiency of SiC is only 1/10 of that of the amorphous carbon,[25] the strong D and G bands do not imply an extremely large amount of amorphous carbon phase in the films. A broad peak positioning at ∼900 cm^{-1} is attributed to the Si−C rocking in Si-CH$_3$.[26−29] The existence of the C−H bonding in the film has been confirmed by the secondary ion mass spectrometry (SIMS) measurement in our previous studies.[14] Such an observation indicates the presence of the amorphous SiC phase in both films.[26−29] However, these three peaks completely disappear in the epitaxial 3C-SiC film. This result indicates strongly that no amorphous phase is incorporated into the epitaxial 3C-SiC film. In other words, the epitaxial 3C-SiC film is composed solely by 3C-SiC crystal. A shift in the position of the SiC TO peak is also observed for the samples. It shifts to lower wavenumbers for the micro- and nanocrystalline 3C-SiC films in comparison with that of the epitaxial 3C-SiC film, indicating their reduced crystallinity. However, a slight upshift of the SiC TO peak of nanocrystalline SiC film in comparison with that of the microcrystalline SiC film also presents, reasonably due to the different stress levels in the films. This is because the nanocrystalline SiC film contains more amorphous phase whose thermal expansion coefficient is different to that of the 3C-SiC crystallites. Moreover, the thickness of the nanocrystalline SiC film is different from that of the microcrystalline SiC film, too. These factors lead to the different stress levels in the nanocrystalline 3C-SiC film, which cause the upshift of its Raman peak in comparison to that of the microcrystalline 3C-SiC.

To get deep insight into the microscopic structures of those films, their transmission electron microscopic (TEM) images were recorded. Those images are shown in Figure 3. The
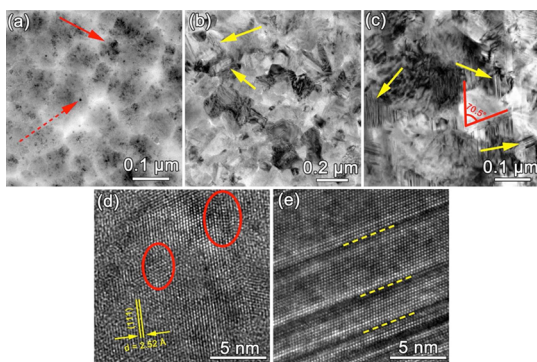

Figure 3. (a−c) Low-magnification TEM images of (a) nanocrystalline, (b) microcrystalline, and (c) epitaxial 3C-SiC films; (d, e) HRTEM images of one typical 3C-SiC crystal in (d) nanocrystalline and (e) microcrystalline 3C-SiC films. The red arrows indicate the 3C-SiC crystals with different sizes in the nanocrystalline 3C-SiC film, the yellow arrows indicate the existence of planar defects in the microcrystalline and epitaxial 3C-SiC films, the circles in d denote the existence of planar defects, and the dashed lines in e indicate the position of planar defects.

differences in crystal size of the films are clearly seen even from their low magnification TEM images in Figure 3a-c. For the nanocrystalline 3C-SiC film (Figure 3a), two kinds of crystals present but with significant differences in their sizes. As indicated by the red arrows, the small crystals feature a size of ∼5 nm whereas the large ones are tens of nanometers in size. The crystals were further confirmed to be 3C-SiC crystals by the high-resolution TEM (HRTEM) measurement in Figure

3d. The typical lattice fringes of 3C-SiC with the interplanar spacing of its {111} planes being 0.252 nm are observed. Moreover, a certain amount of planar defects (twins and stacking faults) exists in the crystal, too. Those twins and stacking faults lie parallel to the {111} planes, as denoted by the red circle in Figure 3d. Regardless of their higher crystallinity, planar defects are also observed in the microcrystalline (Figure 3b) and epitaxial 3C-SiC (Figure 3c) films. Some of them are marked by the yellow arrows in the images. Figure 3e shows the HRTEM image of one typical 3C-SiC microcrystal with planar defects, whose positions are indicated by the dashed lines. The formation of planar defects is actually difficult to be avoided and thus a very common phenomenon during the growth of various SiC structures.[23,30] This is because of their low formation energy. During growth, the energy generated by the mismatch (i.e., lattice mismatch, thermal expansion coefficient mismatch, etc.) between the SiC film and the substrate is sufficient to trigger their formation, leading to their high concentration in the crystals. The cross-sectional TEM image of the epitaxial 3C-SiC film is shown in Figure S2 in the Supporting Information. Even though the existence of the planar defects is also clearly observable throughout the whole film, no small angle grain boundaries exist in the film, indicating that the epitaxial 3C-SiC film can be viewed as a single 3C-SiC crystal but with a high density of planar defects. Such a result is in good accordance with the Raman observation, in which the epitaxial 3C-SiC film is composed solely by the 3C-SiC crystal without any amorphous phase.

From the above structural characterization, it is reasonable for us to conclude that (1) there are significant differences in the film compositions: the nanocrystalline and microcrystalline 3C-SiC films are composed by amorphous carbon, amorphous SiC, and 3C-SiC crystallites, while the epitaxial 3C-SiC film is composed solely by 3C-SiC crystallites; (2) large differences in crystal size exist between the nanocrystalline 3C-SiC film and
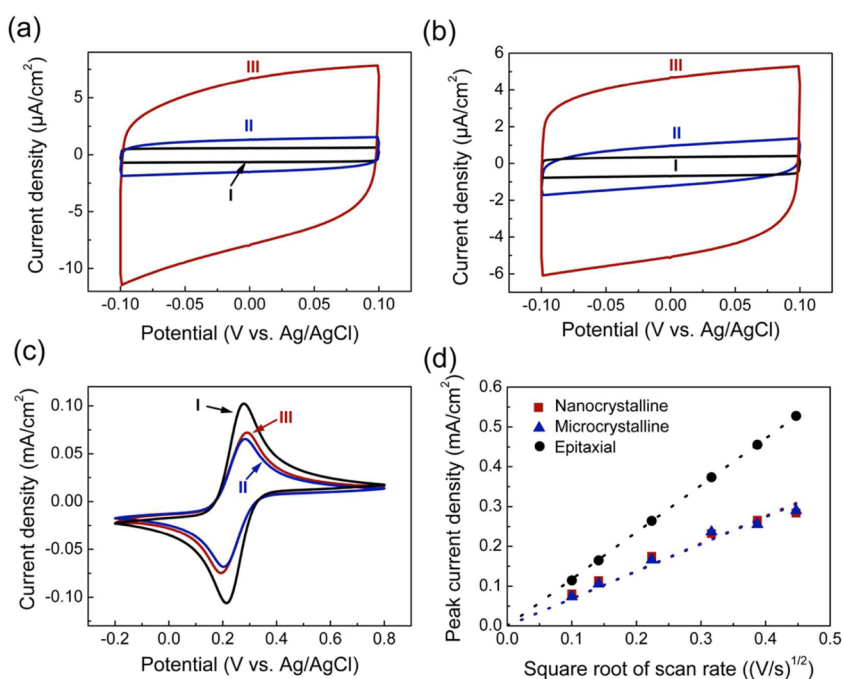

Figure 4. CV of (I) epitaxial, (II) microcrystalline, and (III) nanocrystalline 3C-SiC films at a scan rate of 100 mV/s in the solution of (a) 0.1 M H$_2$SO$_4$; (b) 0.1 M TBABF$_4$ in acetonitrile; (c) 1 mM [Fe(CN)$_6$]$^{3−/4−}$ in 0.1 M KCl. (d) peak current density vs the square root of scan rate in [Fe(CN)$_6$]$^{3−/4−}$. Here, all the current densities are normalized to the geometrical area of the electrodes.

the microcrystalline 3C-SiC film; (3) both the nanocrystalline and microcrystalline 3C-SiC films are polycrystalline, while the epitaxial 3C-SiC film shows perfect (001) orientation; and (4) a large number of planar defects are incorporated in the 3C-SiC crystals in all the films. Please note that the structural information here is only qualitatively discussed. Because the films show significant differences between each other, such a qualitative study is sufficient to distinguish them and draw the main conclusions in the present study.

3.2. Properties of the SiC Films. The significant differences in the composition and crystal size of the above films could have a drastic influence on the properties of the films. In the following, the correlation between the structure and the properties of the films was investigated. We paid more attention to their electrochemical properties.

Prior to electrochemical experiments, the electrical conductivities of those films were measured by four-point-probe technique. The results are summarized in Table 1. Both of the nanocrystalline and microcrystalline 3C-SiC films possess a sheet resistance of ∼3300 Ω/sq, whereas the epitaxial 3C-SiC film shows a much lower sheet resistance of 86 Ω/sq. In the view of electrical conductivity, all films are thus suitable to be applied as the electrodes for electrochemical experiments.

Please note that all the films used in the present study were undoped. Their conductivity is attributed to the existence of defects in the films, i.e., planar defects, grain boundaries and the amorphous phase, as evidenced from the TEM and Raman results. According to Song et al.'s experimental investigation[31] and Tsuboi et al.'s theoretical calculation,[32] the planar defects in 3C-SiC have high electrical conductivity, which is even higher than that of the heavily nitrogen doped (5×10^{18} cm^{-3}) 3C-SiC layers. The amorphous phases, however, show low electrical activity.[33,34] Even though the nanocrystalline and microcrystalline 3C-SiC films contain significant amount of planar defects, the existence of amorphous phases at the grain boundaries could resist the passage of the electric current between the SiC crystals, increasing their resistivity. In contrast, the epitaxial 3C-SiC film is free of the amorphous phases. In addition, antiphase boundaries normally exist at the boundaries between the (001)-oriented SiC crystals, which could further give a rise to its electrical conductivity, making the film even metallically conductive.[35] In this context, the epitaxial 3C-SiC film presents a higher electrical conductivity in comparison with the nanocrystalline and microcrystalline 3C-SiC films.

The electrochemical properties of the films were characterized using cyclic voltammetry. The double layer capacitances of the 3C-SiC films were first evaluated in both aqueous solution (0.1 M H_2SO_4) and nonaqueous solution (0.1 M tetrabutylammonium tetrafluoroborate (TBABF$_4$) in acetonitrile). Figure 4a, b shows the voltammograms at a scan rate of 100 mV/s. The background currents of the epitaxial 3C-SiC film at 0 V were measured to be 0.63 μA/cm^2 in aqueous solution and 0.52 μA/cm^2 in nonaqueous solution. Its double layer capacitances (C, μF/cm^2) were calculated by using the equation of $C = j/\nu$ (j is background current density in μA/cm^2 and ν is scan rate in V/s). They were 6.3 μF/cm^2 and 5.2 μF/cm^2 in aqueous and nonaqueous solutions, respectively, as summarized in Table 2. These values are close to those of the heavily boron doped diamond electrode (2.1−4.5 μF/cm^2), hinting the possibility to adopt the epitaxial 3C-SiC film as the electrode for electrochemical analytical applications. Higher capacitance values of 14.2 μF/cm^2 in the aqueous solution and 10.9 μF/cm^2 in the nonaqueous solution were obtained for the

Table 2. Double-Layer Capacitances of the 3C-SiC Films^a

film type	aqueous		nonaqueous	
	C_{dl} geometrical (μF/cm^2)	C_{dl} real (μF/cm^2)	C_{dl} geometrical (μF/cm^2)	C_{dl} real (μF/cm^2)
nanocrystalline	72.7	56.8	48.5	37.9
microcrystalline	14.2	10.8	10.9	8.3
epitaxial	6.3	5.4	5.2	4.5

^{a}The values are obtained based on the CV curve in Figure 4a, b.

microcrystalline 3C-SiC film (Table 2). Taking into consideration of the surface roughness of the films (estimated from the AFM measurement in Figure 1d-e), the specific double layer capacitance over the real surface area was also evaluated and is shown in Table 2. The specific capacitances of the microcrystalline 3C-SiC film are twice as high as those of the epitaxial 3C-SiC film. Among all 3C-SiC films studied, the nanocrystalline 3C-SiC film possesses the highest double layer capacitances of 72.7 μF/cm^2 in aqueous solution and 48.5 μF/cm^2 in nonaqueous solution (corresponding to 56.8 and 37.9 μF/cm^2 while taking into consideration the real surface area). Please note that slight variations in the deposition conditions of the nanocrystalline 3C-SiC films result in a change in their double-layer capacitances. As shown in Figure S3a in Supporting Information, their double layer capacitances are in the range from ∼40 to ∼100 μF/cm^2, with an average value of 70 μF/cm^2. In contrast to nanocrystalline 3C-SiC film, the double-layer capacitances of the microcrystalline and epitaxial 3C-SiC films exhibit much narrower distribution (Figure S3b, c in the Supporting Information). Nevertheless, because of the high specific capacitance of the nanocrystalline SiC film, its application for super capacitor applications is already promising (see the discussions below in the performance part).

The electrochemical activity of the 3C-SiC films was further examined by using redox probes of $[\text{Fe}(\text{CN})_6]^{3-/4-}$ or $[\text{Ru}(\text{NH}_3)_6]^{2+/3+}$ in aqueous solutions as well as ferrocene and quinone in nonaqueous solutions. Figure 4c shows the exemplary cyclic voltammograms (CV) of $[\text{Fe}(\text{CN})_6]^{3-/4-}$ on the 3C-SiC films. CVs of other redox probes are shown in Figure S4 in the Supporting Information. Well-defined redox waves are clearly observable in all cases. The ΔE_p (peak difference of the anodic peak potential from the cathodic peak potential), $E_p - E_{p/2}$ (the peak differences of anodic/cathodic peak from its half-peak potential) and the dependence of peak currents on the square root of the scan rate (i_p vs $\nu^{1/2}$) in all cases were plotted and estimated, as summarized in Table 3. For all SiC films, the peak currents are proportional to the square root of the scan rate (see Figure 4d and Figure S5 in the Supporting Information), indicating that the electrode process of those redox probes is controlled by their diffusion. Judging from the values of ΔE_p and $E_p - E_{p/2}$, one can tell that the reversibility of the redox probes on all films based electrodes is higher in aqueous solutions in comparison with that in the nonaqueous solutions. Comparing the ΔE_p and $E_p - E_{p/2}$ of the same redox probe on different electrodes leads to the conclusion that the best reversibility of redox probes is on the epitaxial 3C-SiC film and the worst reversibility of redox probes is on the nanocrystalline 3C-SiC film.

It is known that the differences in the reversibility of the redox probes originate from their different charge transfer rates on different substrates. To shed deeper light on this issue, impedance analysis was conducted on all SiC electrodes. The

Table 3. Electrochemical Behavior of Different Redox Probes on Different 3C-SiC Films

film type	redox probes	ΔE (mV)	$E_p - E_{p/2}$ (mV)	linearity of i_p with $\nu^{1/2}$
nanocrystalline	$[Fe(CN)_6]^{3-/4-}$	96	69	√
	$[Ru(NH_3)_6]^{2+/3+}$	88	68	√
	quinone	141	85	√
	ferrocene	150	85	√
microcrystalline	$[Fe(CN)_6]^{3-/4-}$	79	64	√
	$[Ru(NH_3)_6]^{2+/3+}$	81	65	√
	quinone	126	81	√
	ferrocene	143	82	√
epitaxial	$[Fe(CN)_6]^{3-/4-}$	63	59	√
	$[Ru(NH_3)_6]^{2+/3+}$	69	59	√
	quinone	83	66	√
	ferrocene	127	80	√

corresponding impedance spectra are shown in Figure S6 in the Supporting Information. The lowest charge transfer resistance is about 580 Ω obtained on the epitaxial 3C-SiC film based electrode and the highest value is about 3300 Ω obtained on the nanocrystalline 3C-SiC film-based electrode. The low charge transfer resistance of the epitaxial 3C-SiC film leads to the best reversibility of redox probes on it during the cyclic voltammentric measurements.

It is well-understood that surface conditions of the electrode (e.g., the crystal orientation, composition, surface functional groups, etc.) drastically affect the formation of double layer and charge transfer in an electrochemical process.[36,37] In the present study, the epitaxial 3C-SiC film shows high phase purity and perfect (001) crystal orientation (see XRD and Raman measurements). As a result, its properties are expected to be the closest to those of perfect single-crystalline 3C-SiC among all

films in the present study. The microcrystalline 3C-SiC film, however, has a different film composition. It contains not only SiC crystals but also a significant amount of amorphous phases. Moreover, the SiC crystals in the microcrystalline 3C-SiC film are randomly oriented with a large amount of grain boundaries in the film. All these factors lead to a higher heterogeneity at the micrometer scale in the microcrystalline 3C-SiC film in comparison to the epitaxial 3C-SiC film. They influence the overall properties of the film, leading to their deviation from the epitaxial 3C-SiC film. As a result, an increase in the double-layer capacitance and slower charge transfer of the redox reactions on the microcrystalline 3C-SiC films are observed. An even higher degree of heterogeneity is expected in the nanocrystalline 3C-SiC film, because a wider range of distribution in the size of 3C-SiC crystals (from ~5 nm to tens of nanometers) as well as more grain boundaries and amorphous phases (due to the decreased size of the 3C-SiC crystals) present, resulting in a further increase in its double layer capacitance and irreversibility of the redox behavior on its surface.

All the above results clearly indicate that, by engineering their microstructure (crystallinitiy, defects and composition), tunable electrochemical properties of the 3C-SiC films are achieved.

3.3. Performance of the SiC Films. Because of the tunable electrochemical behaviors of the SiC films, they can be designed to suit varieties of electrochemical applications. In the following, the performance of 3C-SiC in two kinds of applications, namely super capacitor (using nanocrystalline 3C-SiC film) and electrochemical sensor (using epitaxial 3C-SiC film), are investigated in detail.

3.3.1. Supercapacitor. The nanocrystalline 3C-SiC film is expected to be a promising candidate for super capacitor applications, since it shows a relatively high double layer capacitance (40−100 $\mu F/cm^2$, depending on the growth
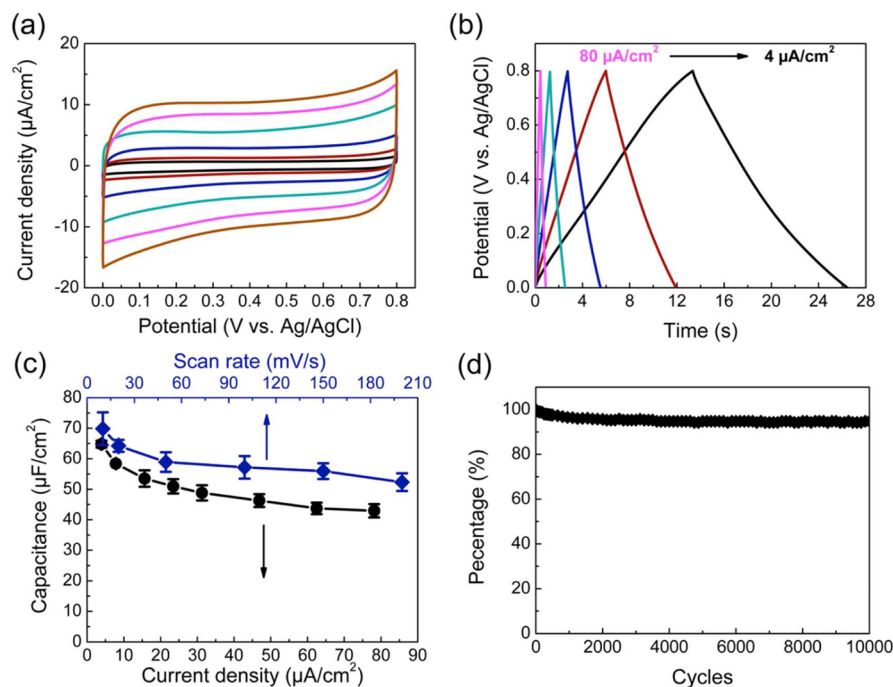

Figure 5. Capacitive behavior of nanocrystalline 3C-SiC film: (a) CV curves in 0.1 M H_2SO_4 with different scan rates, from inside to outside: 10−200 mV/s; (b) charge−discharge curves in 0.1 M H_2SO_4 with different charging current densities; (c) specific capacitances of the film vs scan rate and charging current density; (d) capacitance vs charge−discharge cycles. Here, all the current densities are normalized to the real surface area of the electrodes.

conditions). In order to further confirm this, the capacitive behavior of the nanocrystalline 3C-SiC film shown in Figure 1a was characterized. It has to be pointed out that the current density and the capacitance in the following measurements have been normalized to the real electrode area based on the AFM measurement (Figure 1d).

Figure 5a depicts the CV curves of the nanocrystalline 3C-SiC film in 0.1 M H_2SO_4 at scan rates from 10 to 200 mV/s. For all the scan rates considered, quasi-rectangular shape of the CV curve is clearly observable in the potential range scanned. The CV curve is symmetric, as expected for a typical characteristic of a capacitor. The charge−discharge behavior at different charge/discharge current densities (4 to 80 μA/cm^2) is shown in Figure 5b. For all current densities tested, the anodic charging segment is symmetric to the cathodic discharging counterparts, indicating the high reversibility of its capacitive behavior. The specific capacitance was thus calculated from the CV curves ($C = j/\nu$, j is the background current density in μA/cm^2 and ν is the scan rate in V/s) and the charge−discharge curves ($C = j\Delta t/\Delta V$, j is the charging current density in μA/cm^2, ΔV is the potential range in V and Δt is the charging time in s). As shown in Figure 5c, the highest specific capacitance reaches 70 μF/cm^2 at a scan rate of 10 mV/s. The same as other capacitors, its specific capacitance decreases with an increase of the scan rate or charging current density. Nevertheless, only 34% reduction of its capacitance is observed even with 20-fold increase of the scan rate. In the case of charging current density, the specific capacitance decreases by only 25% (from 65 μF/cm^2 with a charging current density of 4 μA/cm^2 to 43 μF/cm^2 with a charging current density of 80 μA/cm^2). Therefore, an excellent rate capability has been achieved on the nanocrystalline 3C-SiC film. In addition to its high specific capacitance, the cyclic stability of this capacitor, another important factor in evaluating a capacitor, was examined. As shown in Figure 5d, the nanocrystalline 3C-SiC retains 94.8% capacitance after 10 000 cycles. Such a result is comparable with the ones obtained using carbon for super-capactior applications (>80%),[38,39] indicating a very high cyclic stability of the nanocrystalline 3C-SiC electrode.

Table 4 lists specific electrical double layer capacitances (normalized to the real surface area) of several different materials (none pseudocapacitive materials) currently applied frequently for supercapacitor applications. Among them, the electrode based on the nanocrystalline 3C-SiC film shows the highest specific capacitance. Normally during the fabrication of supercapactiors, the positive and negative electrodes as well as their separator are together rolled or folded into a cylindrical or rectangular shape.[52] In this context, the usage of thin nanocrystalline 3C-SiC films with high geometrical specific capacitance would be beneficial in minimizing the device size. Moreover, the capacitance of SiC can be further improved via integrating its surface with metal oxides or conducting polymers. It is already reported that coating SiC nanowires with $Ni(OH)_2$ and MnO_2 can improve the specific capacitance to 1724 and 273.2 F/g, respectively.[53,54] Combining these with its high cyclic stability, nanocrystalline 3C-SiC film is a very promising candidate for the construction of stable, reversible and long lifetime capacitors. To fabricate useful supercapacitor device from the nanocrystalline 3C-SiC film, however, more efforts need be taken in the future. For example, the active surface area of the nanocrystalline 3C-SiC film needs to be increased via introducing pores as well as by rolling-up of very

Table 4. Specific Capacitances of the Typical Materials Used for Double-Layer Capacitor Applications^a

electrode material	electrolyte	double-layer capacitance (real surface area) (μF/cm^2)	refs
activated carbon	30% KOH	15−20	40, 41
	1 M H_2SO_4	10−14	41
pyrolytic graphite	0.9 M NaF	20−70	42, 43
carbon black^b	0.1 M HCl	<10	44
carbide derived porous carbon	ionic liquid	7−14	45, 46
graphene	6 M KOH	2.5−12.5	47
diamond^c	0.1 M H_2SO_4	4	48
Pt^d	1 M H_2SO_4	17−30	49
Au^d	0.5 M H_2SO_4 or $HClO_4$	15−60	50
SiC film^e	3.5 M HCl	6.3	51
nanocrystalline 3C-SiC	0.1 M H_2SO_4	43−70	this work

^{a}All the capacitances listed are normalized to the real surface area. ^{b}Also in 0.1 M NaF and 0.1 M NaOH solutions. ^{c}Also in 0.1 M KCl, 0.1 M NaF and 0.1 M $NaNO_3$ solutions. ^{d}The capacitance values are highly dependent on the potential; metal oxides readily form at high positive potentials. ^{e}The polytype of the SiC film is not mentioned in the literature.

thin freestanding 3C-SiC films (<20 nm thickness), which is currently being undertaken in our laboratory.

3.3.2. Electrochemical Dopamine Sensor. The epitaxial 3C-SiC film has shown a low background current and good reversibility for the redox probes in aqueous solutions. Combining these properties with its good chemical and mechanical stability as well as its good biocompatibility, it could be a potential candidate for electrochemical and biomedical sensor applications, e.g., for in vivo testing.

We have thus chosen dopamine, a common neurotransmitter in the human brain, for a proof-of-concept experiment to elucidate the performance of epitaxial 3C-SiC film in electrochemical sensor applications. Figure 6a shows the voltammetric behavior of 100 μM dopamine on epitaxial 3C-SiC film at different scan rates. The experiment was conducted in a phosphate buffer solution (pH 7.4). Well-defined oxidation peak are observed at 0.4 V, which does not appear in the blank buffer. A small reduction peak is observable at ~0 V, indicating irreversible redox behavior of dopamine on the SiC surface. An increase in the scan rate leads to an enhancement of the peak current density. Figure 6b presents the proportional relationship between the peak current and the square root of scan rate, implying that the oxidation of dopamine on the SiC electrode is a diffusion-controlled process, instead of an adsorption-controlled one. Consequently, dopamine is irreversibly oxidized on the epitaxial 3C-SiC film based electrode and the sensing of dopamine on the epitaxial 3C-SiC film is thus possible to be achieved.

Differential pulse voltammetry (DPV) were adopted for the sensing of dopamine. Figure 6c shows the DPV of dopamine at different concentrations after optimization of the detection conditions. The anodic peak current density, $j_{p,a}$, shows linear relationship with the concentration of dopamine, c, in the concentration range of 2−200 μM. As shown in Figure 6d, the linear regression equation is expressed as $j_{p,a}$ (μA/cm^2) = (−0.34) + 0.068c (μM). The coefficient factor is 0.998 (n = 9). The detection limit was determined to be 0.7 μM or 0.1 mg/L (based on S/N = 3 of 7 measurements in the solution
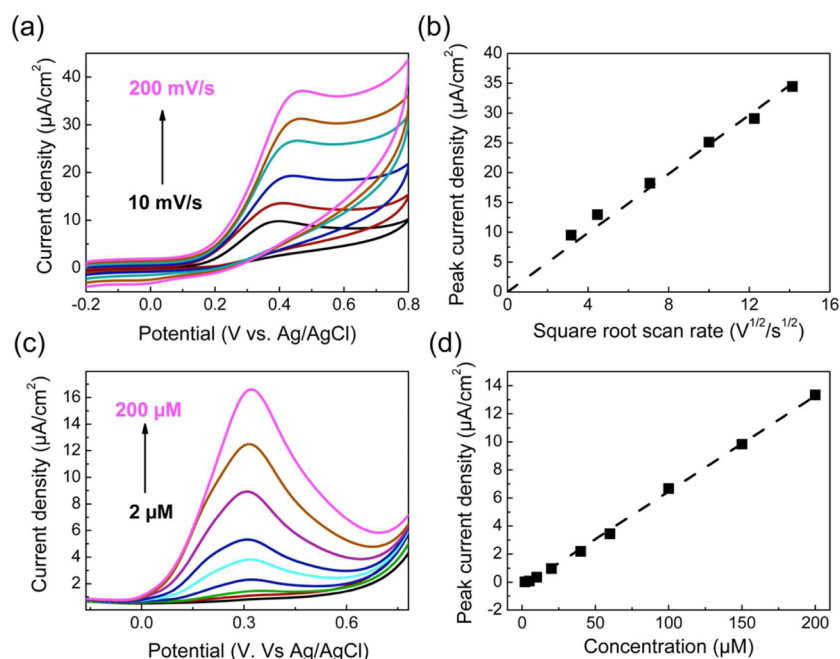
Figure 6. Dopamine sensing using epitaxial 3C-SiC film: (a) CV curves in 100 μM dopamine with different scan rates; (b) peak current density in the CV curve vs square root of scan rate; (c) DPV curves of dopamine with different concentrations; (d) peak intensity in the DPV curve vs concentration. Here, the current densities are normalized to the geometrical area of the electrodes.

containing 10 μM dopamine). Although the limit-of-detection (LOD) of epitaxial 3C-SiC film is not as low as that obtained on other electrodes reported in literature,[55] the workable concentration range for dopamine detection on the SiC electrode is still one to two orders lower than its concentration in tissue (4−10 mg/L).[56,57] Therefore, the SiC film-based electrode is suitable and promising as an electrochemical sensor for biomedical sensing of biomolecules (i.e., dopamine). Future investigations are needed to fabricate SiC based dopamine sensor, for example, the interference study of other molecules such as uric acid and ascorbic acid as well as the in vivo testing. These activities are of great importance and form the aim of our future study on the electrochemical applications of the SiC films.

4. CONCLUSIONS

The structure and the electrochemical properties of different 3C-SiC films have been studied. The relationship between their microstructures (e.g., crystallinitiy, defects, and phase composition) and their electrochemical properties has been discussed in detail. The differences in their microstructures result in their different electrochemical behaviors. For example, the epitaxial 3C-SiC film shows the lowest double layer capacitance and the highest reversibility of redox probes; the nanocrystalline SiC film shows extremely high double-layer capacitance with only quasi-reversible behavior of the redox probes. The structural heterogeneity is considered as the main reason for the different electrochemical behaviors. On the basis of their different electrochemical properties, their performances in two different applications, namely supercapacitor and electrochemical sensor for dopamine detection, have been demonstrated using nanocrystalline 3C-SiC film and epitaxial 3C-SiC film, respectively. Future works are still needed to focus on the structuring of those films with aid of nanotechnology as well as their further surface modification to improve and broaden their applications.

■ ASSOCIATED CONTENT

ⓢ Supporting Information

SEM and TEM cross-sectional images of the 3C-SiC films, cyclic voltammetry and peak intensity vs square root of scan rate of ferrocene, quinone and $[Ru(NH_3)_6]^{2+/3+}$ on different 3C-SiC films, and impedance analysis of different 3C-SiC films. The Supporting Information is available free of charge on the ACS Publications website at DOI: 10.1021/acsami.5b02024.

■ AUTHOR INFORMATION

Corresponding Author

*E-mail: xin.jiang@uni-siegen.de. Tel: +49 271 740 2966. Fax: +49 271 740 2442.

Notes

The authors declare no competing financial interest.

■ ACKNOWLEDGMENTS

■ REFERENCES

(1) Callister, W. D.; Rethwisch, D. G. *Materials Science and Engineering: An Introduction*, 8th ed.; John Wiley & Sons: New York, 2009.

(2) Yang, W. S.; Auciello, O.; Butler, J. E.; Cai, W.; Carlisle, J. A.; Gerbi, J.; Gruen, D. M.; Knickerbocker, T.; Lasseter, T. L.; Russell, J. N.; Smith, L. M.; Hamers, R. J. DNA-Modified Nanocrystalline Diamond Thin-Films as Stable, Biologically Active Substrates. *Nat. Mater.* **2002**, *1*, 253−257.

(3) Zhuang, H.; Srikanth, V. V. S. S.; Jiang, X.; Luo, J.; Ihmels, H.; Aronov, I.; Wenclawiak, B. W.; Adlung, M.; Wickleder, C. Allylamine-Mediated DNA Attachment to Polycrystalline Diamond Surface. *Appl. Phys. Lett.* **2009**, *95*, 143703.

(4) Gaebel, T.; Domhan, M.; Popa, I.; Wittmann, C.; Neumann, P.; Jelezko, F.; Rabeau, J. R.; Stavrias, N.; Greentree, A. D.; Prawer, S.; Meijer, J.; Twamley, J.; Hemmer, P. R.; Wrachtrup, J. Room-

Temperature Coherent Coupling of Single Spins in Diamond. *Nat. Phys.* **2006**, *2*, 408−413.

(5) Bernius, M. T.; Inbasekaran, M.; O'Brien, J.; Wu, W. Progress with Light-Emitting Polymers. *Adv. Mater.* **2000**, *12*, 1737−1750.

(6) *Carbide, Nitride and Boride Materials Synthesis and Processing*; Weimer, A. W., Ed.; Chapman & Hall: London, 1997.

(7) Anthony, L. J. Sublimation Process for Manufacturing Silicon Carbide Crystals. U.S. 2854364A, September 30, 1958.

(8) *Properties of Silicon Carbide*; Harris, G. L., Ed.; Short Run Press: Exeter, U.K., 1995.

(9) Godignon, P. In *Silicon Carbide and Related Materials 2004*; Nipoti, R., Poggi, A., Scorzoni, A., Eds.; Trans Tech Publications: Pfaffikon, Switzerland, 2005; Vol. 483, pp 1009−1014.

(10) Wright, N. G.; Horsfall, A. B. SiC Sensors: a Review. *J. Phys. D: Appl. Phys.* **2007**, *40*, 6345−6354.

(11) Yakimova, R.; Petoral, R. M., Jr.; Yazdi, G. R.; Vahlberg, C.; Spetz, A. L.; Uvdal, K. Surface Functionalization and Biomedical Applications Based on SiC. *J. Phys. D: Appl. Phys.* **2007**, *40*, 6435−6442.

(12) Frewin, C. L.; Reyes, M.; Register, J.; Thomas, S. W.; Saddow, S. E. 3C-SiC on Si: A Versatile Material for Electronic, Biomedical and Clean Energy Applications. *MRS Online Proc. Libr.* **2014**, *1693*, DOI: 10.1557/opl.2014.567.

(13) Yang, N.; Zhuang, H.; Hoffmann, R.; Smirnov, W.; Hees, J.; Jiang, X.; Nebel, C. E. Nanocrystalline 3C-SiC Electrode for Biosensing Applications. *Anal. Chem.* **2011**, *83*, 5827−5830.

(14) Yang, N.; Zhuang, H.; Hoffmann, R.; Smirnov, W.; Hees, J.; Jiang, X.; Nebel, C. E. Electrochemistry of Nanocrystalline 3C Silicon Carbide Films. *Chem.—Eur. J.* **2012**, *18*, 6514−6519.

(15) Zhuang, H.; Wang, C.; Huang, N.; Jiang, X. Cubic SiC for Trace Heavy Metal Ion Analysis. *Electrochem. Commun.* **2014**, *41*, 5−7.

(16) Zhuang, H.; Zhang, L.; Staedler, T.; Jiang, X. Low Temperature Hetero-Epitaxial Growth of 3C-SiC Films on Si Utilizing Microwave Plasma CVD. *Chem. Vap. Deposition.* **2013**, *19*, 29−37.

(17) Lin, H.; Gerbec, J. A.; Sushchikh, M.; McFarland, E. W. Synthesis of Amorphous Silicon Carbide Nanoparticles in a Low Temperature Low Pressure Plasma Reactor. *Nanotechnology* **2008**, *19*, 325601.

(18) Zhuang, H.; Zhang, L.; Staedler, T.; Jiang, X. Nanoscale Integration of SiC/SiO$_2$ Core-Shell Nanocables in Diamond through a Simultaneous Hybrid Structure Fabrication. *Appl. Phys. Lett.* **2012**, *100*, 193102.

(19) Zhuang, H.; Zhang, L.; Fuchs, R.; Staedler, T.; Jiang, X. When Epitaxy Meets Plasma: a Path to Ordered Nanosheets Arrays. *Sci. Rep.* **2013**, *3*, 2427.

(20) Yu, M.; Jayanthi, C. S.; Wu, S. Y. Size-, Shape-, and Orientation-Dependent Properties of SiC Nanowires of Selected Bulk Polytypes. *J. Mater.Res.* **2013**, *28*, 57−67.

(21) Cheng, G.; Chang, T.-H.; Qin, Q.; Huang, H.; Zhu, Y. Mechanical Properties of Silicon Carbide Nanowires: Effect of Size-Dependent Defect Density. *Nano Lett.* **2014**, *14*, 754−758.

(22) Zhuang, H.; Song, B.; Srikanth, V. V. S. S.; Jiang, X.; Schönherr, H. Controlled Wettability of Diamond/β-SiC Composite Thin Films for Biosensoric Applications. *J. Phys. Chem. C* **2010**, *114*, 20207−20212.

(23) Nagasawa, H.; Yagi, K.; Kawahara, T. 3C-SiC Hetero-Epitaxial Growth on Undulant Si(001) Substrate. *J. Cryst. Growth* **2002**, *237−239*, 1244−1249.

(24) Zhuang, H.; Zhang, L.; Staedler, T.; Jiang, X. Highly Selective Diamond and β-SiC Crystal Formation at Increased Atomic Hydrogen Concentration: A Route for Synthesis of High-Quality and Patterned Hybrid Diamond/β-SiC Composite Film. *Scr. Mater.* **2011**, *65*, 548−551.

(25) Sasaki, Y.; Nishina, Y.; Sato, M.; Okamura, K. Raman-Study of SiC Fibers Made from Polycarbosilane. *J. Mater. Sci.* **1987**, *22*, 443−448.

(26) Inoue, Y.; Nakashima, S.; Mitsuishi, A.; Tabata, S.; Tsuboi, S. Raman Spectra of Amorphous SiC. *Solid State Commun.* **1983**, *48*, 1071−1075.

(27) Catherine, Y.; Zamouche, A.; Bullot, J.; Gauthier, M. Ion Bombardment Effects in Plasma Deposition of Hydrogenated Amorphous Silicon Carbide Films: A Comparative Study of D.C. and R.F. Discharges. *Thin Solid Films* **1983**, *109*, 145−158.

(28) Dutta, R.; Banerjee, P. K.; Mitra, S. S. Effect of Hydrogenation on the Electrical Conductivity of Amorphous Silicon Carbide. *Solid State Commun.* **1982**, *42*, 219−222.

(29) Bullot, J.; Schmidt, M. P. Physics of Amorphous Silicon−Carbon Alloys. *Phys. Status Solidi B* **1987**, *143*, 345−418.

(30) Nagasawa, H.; Yagi, K.; Kawahara, T.; Hatta, N. Reducing Planar Defects in 3C−SiC. *Chem. Vap. Deposition* **2006**, *12*, 502−508.

(31) Song, X.; Michaud, J. F.; Cayrel, F.; Zielinski, M.; Portail, M.; Chassagne, T.; Collard, E.; Alquier, D. Evidence of Electrical Activity of Extended Defects in 3C-SiC Grown on Si. *Appl. Phys. Lett.* **2010**, *96*, 142104.

(32) Tsuboi, H.; Kabasawa, M.; Ouchi, S.; Sato, M.; Sahnoun, R.; Koyma, M.; Hatakeyama, N.; Endou, A.; Takaba, H.; Kubo, M.; Del Carpio, C. A.; Kitou, Y.; Makino, E.; Hosokawa, N.; Hasegawa, J.; Onda, S.; Miyamoto, A. Computational Evaluation of Electrical Conductivity on SiC and The influence of Crystal Defects. *Mater. Sci. Forum* **2009**, *600−603*, 497−500.

(33) Dasgupta, D.; Demichelis, F.; Tagliaferro, A. Electrical Conductivity of Amorphous Carbon and Amorphous Hydrogenated Carbon. *Philos. Mag. B* **1991**, *63*, 1255−1266.

(34) Demichelis, F.; Pirri, C. F.; Tresso, E.; Mea, G. D.; Rigato, V.; Rava, P. Physical Properties of Undoped and Doped Hydrogenated Amorphous Silicon Carbide. *Semicond. Sci. Technol.* **1991**, *6*, 1141.

(35) Raffy, C.; Furthmüller, J.; Wagner, J. M.; Bechstedt, F. Ab Initio Study of Structural and Electronic Properties of Planar Defects in Si and SiC. *Phys. Rev. B* **2004**, *70*, 195344.

(36) Lvovich, V. F. *Impedance Spectroscopy with Application to Electrochemical and Dielectric Phenomena*; John Wiley & Sons: New York, 2012.

(37) Bard, A. J.; Larry, R. *Electrochemical Methods: Fundamentals and Applications*; John Wiley & Sons: New York, 2001.

(38) Ania, C. O.; Khomenko, V.; Raymundo-Piñero, E.; Parra, J. B.; Béguin, F. The Large Electrochemical Capacitance of Microporous Doped Carbon Obtained by Using a Zeolite Template. *Adv. Funct. Mater.* **2007**, *17*, 1828−1836.

(39) Zhang, L. L.; Zhao, X. S. Carbon-Based Materials as Supercapacitor Electrodes. *Chem. Soc. Rev.* **2009**, *38*, 2520−2531.

(40) Shi, H. Activated Carbons and Double Layer Capacitance. *Electrochim. Acta* **1996**, *41*, 1633−1639.

(41) Ruiz, V.; Blanco, C.; Raymundo-Piñero, E.; Khomenko, V.; Béguin, F.; Santamaría, R. Effects of Thermal Treatment of Activated Carbon on the Electrochemical Behaviour in Supercapacitors. *Electrochim. Acta* **2007**, *52*, 4969−4973.

(42) Randin, J.-P.; Yeager, E. Differential Capacitance Study on the Basal Plane of Stress-Annealed Pyrolytic Graphite. *J. Electroanal. Chem. Interfacial Electrochem.* **1972**, *36*, 257−276.

(43) Randin, J.-P.; Yeager, E. Differential Capacitance Study on the Edge Orientation of Pyrolytic Graphite and Glassy Carbon Electrodes. *J. Electroanal. Chem. Interfacial Electrochem.* **1975**, *58*, 313−322.

(44) Oren, Y.; Tobias, H.; Soffer, A. The Electrical Double Layer of Carbon and Graphite Electrodes: Part I. Dependence on Electrolyte Type and Concentration. *J. Electroanal. Chem. Interfacial Electrochem.* **1984**, *162*, 87−99.

(45) Largeot, C.; Portet, C.; Chmiola, J.; Taberna, P.-L.; Gogotsi, Y.; Simon, P. Relation between the Ion Size and Pore Size for an Electric Double-Layer Capacitor. *J. Am. Chem. Soc.* **2008**, *130*, 2730−2731.

(46) Chmiola, J.; Yushin, G.; Gogotsi, Y.; Portet, C.; Simon, P.; Taberna, P. L. Anomalous Increase in Carbon Capacitance at Pore Sizes Less Than 1 Nanometer. *Science* **2006**, *313*, 1760−1763.

(47) Ji, H.; Zhao, X.; Qiao, Z.; Jung, J.; Zhu, Y.; Lu, Y.; Zhang, L. L.; MacDonald, A. H.; Ruoff, R. S. Capacitance of Carbon-based Electrical Double-Layer Capacitors. *Nat. Commun.* **2014**, *5*, 3317.

(48) Swain, G. M.; Ramesham, R. The Electrochemical Activity of Boron-Doped Polycrystalline Diamond Thin Film Electrodes. *Anal. Chem.* **1993**, *65*, 345−351.

(49) Rosen, M.; Flinn, D. R.; Schuldiner, S. Double Layer Capacitance on Platinum in 1 M H_2SO_4 from the Reversible Hydrogen Potential to the Oxygen Formation Region. *J. Electrochem. Soc.* **1969**, *116*, 1112−1116.

(50) Germain, P. S.; Pell, W. G.; Conway, B. E. Evaluation and Origins of the Difference between Double-Layer Capacitance Behaviour at Au-Metal and Oxidized Au Surfaces. *Electrochim. Acta* **2004**, *49*, 1775−1788.

(51) Alper, J. P.; Kim, M. S.; Vincent, M.; Hsia, B.; Radmilovic, V.; Carraro, C.; Maboudian, R. Silicon Carbide Nanowires as Highly Robust Electrodes for Micro-Supercapacitors. *J. Power Sources* **2013**, *230*, 298−302.

(52) Simon, P.; Gogotsi, Y. Materials for Electrochemical Capacitors. *Nat. Mater.* **2008**, *7*, 845−854.

(53) Gu, L.; Wang, Y.; Lu, R.; Wang, W.; Peng, X.; Sha, J. Silicon Carbide Nanowires@Ni(OH)$_2$ Core-Shell Structures on Carbon Fabric for Supercapacitor Electrodes with Excellent Rate Capability. *J. Power Sources* **2015**, *273*, 479−485.

(54) Kim, M.; Yoo, Y.; Kim, J. Synthesis of Microsphere Silicon Carbide/Nanoneedle Manganese Oxide Composites and their Electrochemical Properties as Supercapacitors. *J. Power Sources* **2014**, *265*, 214−222.

(55) Smirnov, W.; Yang, N.; Hoffmann, R.; Hees, J.; Obloh, H.; Müller-Sebert, W.; Nebel, C. E. Integrated All-Diamond Ultra-microelectrode Arrays: Optimization of Faradaic and Capacitive Currents. *Anal. Chem.* **2011**, *83*, 7438−7443.

(56) Walsh, F. X.; Stevens, T. J.; Langlais, P. J.; Bird, E. D. Dopamine and Homovanillic Acid Concentrations in Striatal and Limbic Regions of Human Brain. *Ann. Neurol.* **1982**, *12*, 52−55.

(57) Wilk, S.; Stanley, M. Dopamine Metabolites in Human Brain. *Psychopharmacology* **1978**, *57*, 77−81.